PERSPECTIVE

Check for updates

Activatable molecular agents for cancer theranostics

Jianjian Zhang, †*[a] Lulu Ning, †[b] Jiaguo Huang, [c] Chi Zhang [c] and Kanyi Pu *[c]

Theranostics that integrates diagnosis and treatment modalities has attracted great attention due to its abilities of personalized therapy and real-time monitoring of therapeutic outcome. Such a theranostic paradigm requires agents to simultaneously possess the capabilities of targeting, imaging, and treatment. Activatable molecular agents (AMAs) are promising for cancer theranostics, as they show a higher signal-to-noise ratio (SNR), real-time detection of cancer-associated biomarkers, lower normal tissue toxicity, and a higher therapeutic effect. This perspective summarizes the recent advancements of AMAs, which include imaging-guided chemotherapy, imaging-guided photodynamic therapy, and imaging-guided photothermal therapy. The molecular design principles, theranostic mechanisms, and biomedical applications of AMAs are described, followed by a discussion of potential challenges of AMAs in cancer theranostics.

1. Introduction

Cancer, also known as a malignant tumor, is one of the major diseases that threaten people's lives globally.[1] Traditional tumor treatments mainly include surgical resection, chemotherapy, and radiotherapy. However, the unmarked remaining cancer cells after surgical resection easily metastasize, leading to postoperative recurrence. Moreover, chemotherapy and radiotherapy show a significant killing effect on both tumor and normal tissues. Besides, tumor cells are prone to developing resistance to chemotherapy and radiotherapy.[2,3] Therefore, the

[a]Key Laboratory of Synthetic and Natural Functional Molecule Chemistry of Ministry of Education, Key Lab of Modern Separation Science in Shaanxi Province, College of Chemistry and Materials Science, Northwest University, Xi'an, 710127, Shaanxi, P. R. China. E-mail: zhangjj@nwu.edu.cn

[b]Shaanxi Provincial Key Laboratory of Papermaking Technology and Specialty Paper Development, College of Bioresources Chemical and Materials Engineering, Shaanxi University of Science & Technology, Xi'an, 710021, P. R. China

[c]School of Chemical and Biomedical Engineering, Nanyang Technological University, Singapore 637457. E-mail: kypu@ntu.edu.sg

† These authors contributed equally to this work.

Jianjian Zhang received his masters degree (2013) in Organic Chemistry and doctoral degree (2016) in Analytical Chemistry from Lanzhou University. After postdoctoral research in Prof. Kanyi Pu's group at Nanyang Technological University (2016-2017), he worked at Northwest University as an associate professor. His research focuses on the development of activatable molecular probes for tumor imaging.

Kanyi Pu received his PhD from the National University of Singapore in 2011 followed by a postdoctoral study at the Stanford University School of Medicine. He joined the School of Chemical and Biomedical Engineering (SCBE) at Nanyang Technological University (NTU) as an Associate Professor in 2015. He has been named one of the world's most highly cited researchers by the Web of Science. His research lies at the intersection of chemistry, nanotechnology, biophotonics and medicine, aiming to develop smart molecular probes and advanced imaging technologies to understand, detect and treat life-threatening diseases.

combination of timely diagnosis of cancer and effective treatment methods has become a research focus.

Theranostics, a new biomedical technology that combines diagnosis with therapy, has great potential in personalized cancer medicine, including real-time monitoring of the treatment process and reflecting the feedback of the therapeutic effect. So far, great efforts have been devoted to the development of theranostic agents.[4–8] There are two main kinds of strategies. One is to use a chemical synthesis method. Various anticancer molecules, imaging agents and cancer-targeting molecules are covalently conjugated together through chemical reactions, affording macromolecular agents capable of tumor targeting, imaging, and therapy. The other is nanoparticle encapsulation. Imaging agents and anticancer molecules are encapsulated in amphiphilic coatings to form nanoparticles, which can be delivered to the solid tumor through specific targeting or the enhanced permeability and retention (EPR) effect. Numerous theranostic systems combining different imaging techniques (*e.g.*, magnetic resonance imaging (MRI), positron emission tomography (PET), fluorescence imaging (FLI), and photoacoustic imaging (PAI)) with diverse therapeutic methods (including chemotherapy (CHT), photodynamic therapy (PDT), photothermal therapy (PTT), and gene therapy (GT)) through one (imaging)-to-one (therapy), many-to-one, one-to-many, and many-to-many types have been developed.[9–32] Since different modalities can make up for another's limitation, offer improved imaging quality and/or therapeutic efficacy, and minimize the probability of overmedication, the development of a single molecular probe integrated with multimodalities has great potential in the treatment of cancer.

However, most theranostic agents employ an "always-on" mode for both diagnosis and therapeutic intervention, leading to a limited signal-to-noise ratio (SNR) in the disease sites and notable side effects in normal tissues.[33–37] In contrast, activatable theranostic agents capable of intrinsic signal changes with simultaneous initiation of therapeutic activity upon detection of biomarkers (from the "off" state to the "on" state) demonstrate the potential for a higher SNR, a lower limit of detection (LOD), real-time detection of biomarkers, lower normal tissue toxicity, and higher drug bioavailability. However, such an activatable approach is challenging as it requires recognition of reactions that are precisely induced by a single species. Hence, activatable theranostic agents have been far less developed.

Many multi-modality materials have been exploited as theranostic agents, such as upconversion nanoparticles (NPs),[38] carbon nanotubes,[39] gold nanoclusters,[40] reduced graphene oxide,[41] magnetic NPs,[42] quantum dots,[43] semiconducting polymer nanoparticles (SPNs),[23,28,44–49] and small molecule dyes.[9,50–52] Each has its own advantages and shortcomings. For instance, inorganic nanomaterials possess excellent properties of optical tunability and phototherapeutic ability, but their toxicity in clinical applications still needs to be addressed urgently.[53,54] Molecular agents have long been a research focus in life sciences and biomedicine owing to their significant merits, such as a simple and controllable molecular structure,

easy production on a large scale, better biocompatibility, and easy metabolism in living organisms. Hence, distinct breakthroughs and evolvements of theranostics based on AMAs have been achieved during the past few years and could notably accelerate the development of cancer theranostics.

The design strategies of molecule-based theranostic agents with improved therapeutic effects and minimized side effects have been recently reviewed,[4,8,55] some of which have already been used in clinical application for PDT such as porphyrin and 5-aminolevulinic acid and their derivatives.[56–58] Herein, this perspective mainly describes the latest research achievements of AMAs. In the following, we summarize and discuss different therapeutic modalities that have been developed using AMAs (Fig. 1). The design principles, therapeutic mechanisms, and biological applications of these theranostic agents are clearly illustrated. Moreover, a discussion regarding the potential challenges of AMAs is also provided.

2.   Chemotheranostics

Chemotherapy as the main treatment modality for various cancers utilizes chemical drugs such as doxorubicin (DOX),[59] camptothecin (CPT),[60] etoposide,[61] *S*-crizotinib,[62] 7-ethyl-10-hydroxycamptothecin (SN-38),[63] gemcitabine,[64] and paclitaxel[65] to prevent the anabolism of nucleic acids, DNA replication, spindle formation, and protein synthesis. Such inhibition
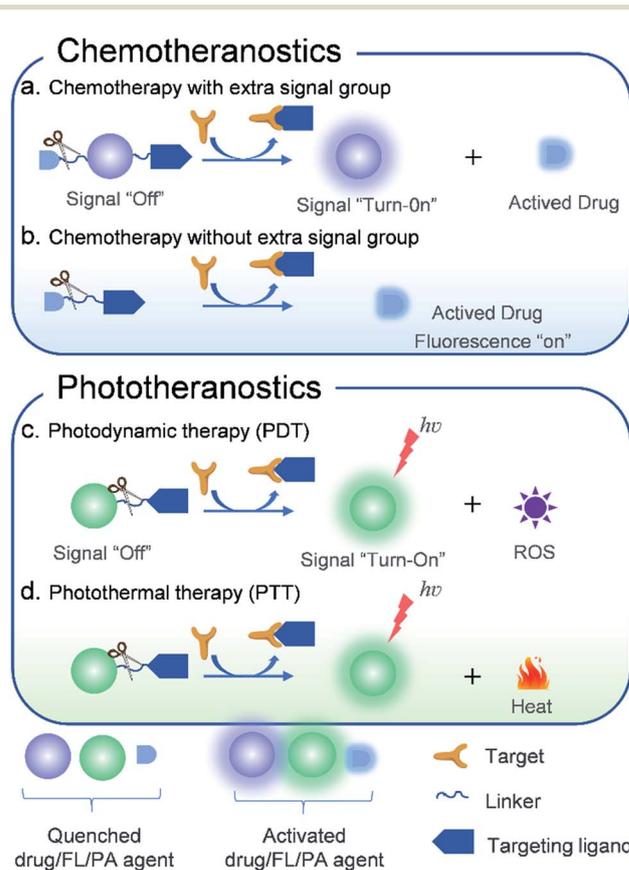

Fig. 1 Schematic illustration of the design principles of activatable molecular agents for CHT, PDT, and PTT.

retards the growth and reproduction of tumor cells, finally destroying cancer cells. Although these current clinical chemotherapeutic agents demonstrate high efficiency in anti-cancer progression, they have serious drawbacks such as poor selectivity towards cancer cells, low drug bioavailability, and high systemic toxicity. To solve these problems, activatable theranostic agents that integrate targeted molecular optical reporters with chemotherapy drugs have been developed by some research groups.[66–68] When interacting with various tumor-associated stimuli (*e.g.*, a highly reactive oxygen species (ROS) level, hypoxia, a highly expressed enzyme, acidity, and reduction), the activatable theranostic agents can precisely kill cancer cells. Meanwhile, the easy-to-monitor signals of the optical reporter also change from "off" to "on". Furthermore, a series of molecule-based theranostic agents with improved therapeutic effects but minimized side effects have recently been developed.

2.1. Fluorescence imaging-guided CHT

The fluorescence imaging technique has become an indispensable tool in biological research due to the versatile emission spectra, non-invasiveness, high temporal and spatial resolution, fast-scanning speed, and real-time monitoring. Encouraged by the high performance of molecular probes in both FLI and CHT, AMAs have widely been used in the application of FLI-guided CHT.[50,67] The platforms can be divided into

three types: (i) drugs connected with a fluorophore through a linker cleavable by a bio-marker; (ii) therapeutic agents with fluorescence features connected with the targeting group through a linker; (iii) both drugs and fluorophore encapsulated in polymers or mesoporous materials.

For instance, based on a multicomponent (fluorophore, drug, linker, and targeting group) synthesis strategy, Kim *et al.*[69] constructed a theranostic agent, RGD peptide-appended naphthalimide pro-camptothecin (RGD-NAP-CPT), for imaging-guided chemotherapy (Fig. 2a). RGD-NAP-CPT was a multifunctional molecule composed of an RGD cyclic peptide as a particularly effective cancer-targeting unit, a naphthalimide fragment as a fluorophore, a disulfide bond as a glutathione (GSH) cleavable linker, and camptothecin (CPT) as an anti-tumor inhibitor of topoisomerase I.[70] The prodrug agent was endocytosed into the targeted cancer cells through the interaction between RGD and an $\alpha_v\beta_3$ integrin receptor. Upon reaction with GSH which is relatively abundant in tumor cells, disulfide cleavage occurred, leading to the release of free cytotoxic CPT in the endoplasmic reticulum, along with naphthalimide which emitted an intense red-shifted fluorescence signal at 535 nm. CPT, in turn, diffused into the nucleus of the cancer cells, inhibiting the activity of topoisomerase I and achieving the anti-tumor effect (Fig. 2b). These results demonstrated that RGD-NAP-CPT could act as a theranostic agent to provide FLI-guided CHT.
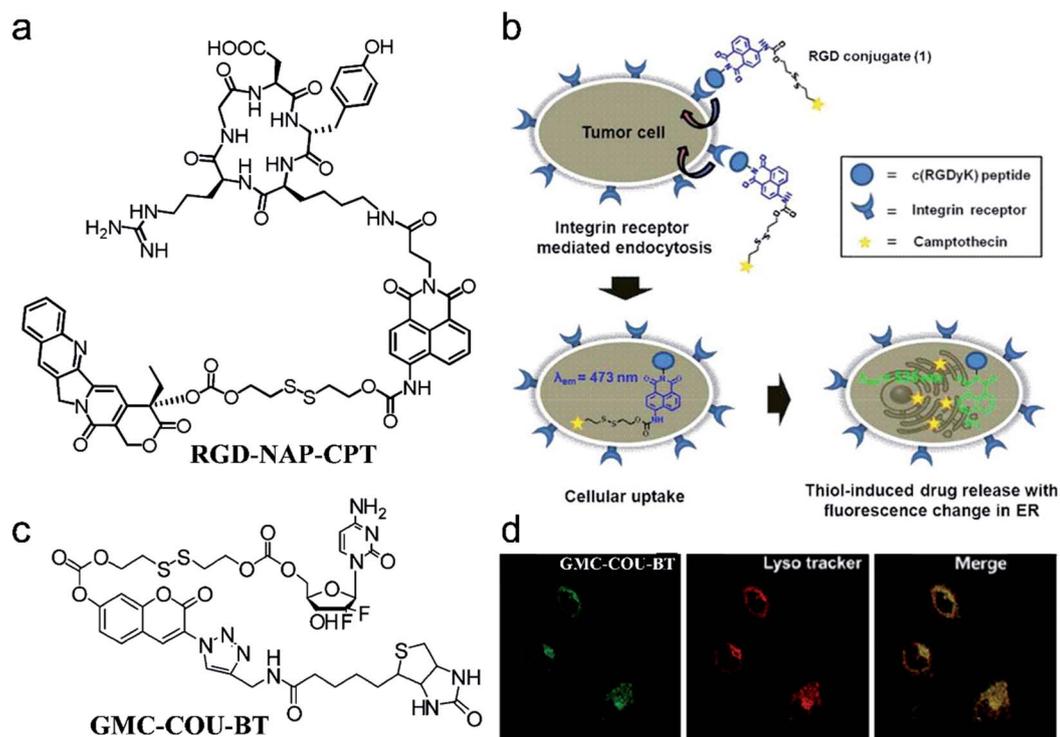

Fig. 2 (a) Structure of the theranostic agent RGD–NAP–CPT. (b) Schematic mode of action of RGD–NAP–CPT in cancer cells. RGD–NAP–CPT is selectively internalized in the cells through receptor-mediated endocytosis. Fluorescence emission and cytotoxicity of the prodrug are activated due to cleavage of the disulfide bond by GSH. Adapted from ref. 66. Copyright 2012 American Chemical Society. (c) Structure of the theranostic agent GMC–COU–BT. (d) Confocal microscopy images of the colocalized experiment in A549 cells. Adapted from ref. 68. Copyright© 2013 American Chemical Society.
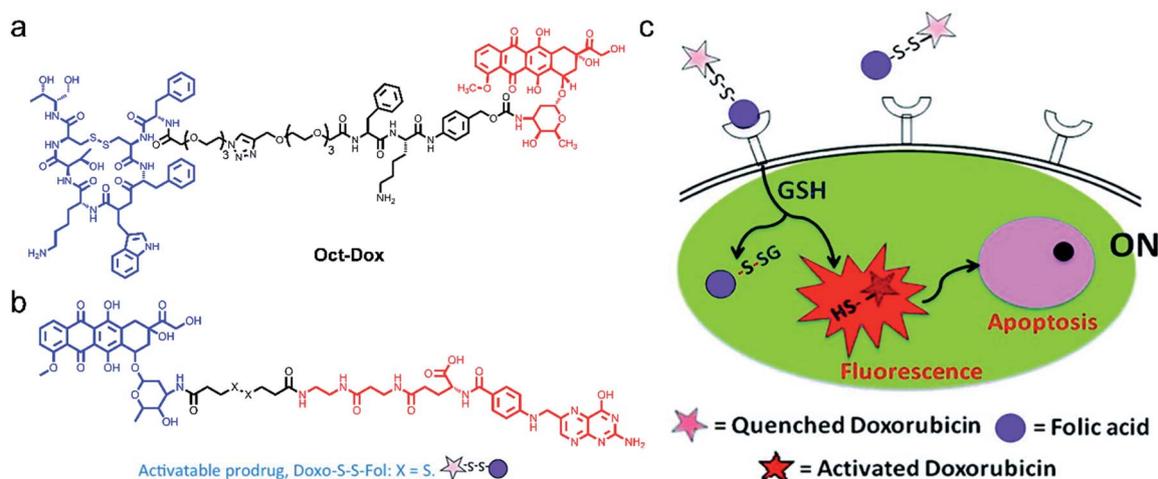
Fig. 3 Structures of Oct-Dox (a) and Doxo-S-S-Fol (b). (c) The schematic illustration of the cancer therapy mechanism of Doxo-S-S-Fol. The fluorescence emission and cytotoxicity of the prodrug (Doxo-S-S-Fol) are quenched (off) in the extra-cellular milieu. Upon target-specific internalization, enhanced fluorescence emission and cytotoxicity (on) occur due to cleavage of the disulfide bond by GSH. Adapted from ref. 63. Copyright© 2011 American Chemical Society.

To illustrate the universality of this strategy, Kim and co-workers[71] prepared a cancer-targeting theranostic smart drug delivery system based on a gemcitabine–coumarin–biotin (GMC–COU–BT) conjugate (Fig. 2c). GMC–COU–BT was composed of a cancer targeting ligand biotin,[72] a thiol-specific cleavable disulfide bond, a coumarin moiety as a fluorescent reporter, and gemcitabine (GMC) as a model active drug. By tracking the green emission of the coumarin molecules, lysosome trapping of GMC followed by drug release into the cell cytoplasm (Fig. 2d) and the distribution of the drug was revealed. Besides, the therapeutic effect of this theranostic agent could easily be monitored at the subcellular level by two-photon fluorescence imaging.

In the development of theranostic agents, the utmost challenge lies in the low specificity and high systemic toxicity. Targeting theranostic agents to cancer cells helps to improve therapeutic efficiency. However, this visualization of targeted drug delivery requires additional fluorescence labelling, which may change the route of the drug molecules. Hence, there is an urgent need to design therapeutic agents with intrinsic fluorescence for guiding and displaying therapeutic effects. Shin et al.[73] developed a dual-targeting therapeutic agent (Oct-Dox) via conjugation of a synthetic ligand (octreotide) of the cancer-selective somatostatin receptor, a peptide substrate that can be cleaved by cathepsin B overexpressed in cancer cells, to an anticancer agent with intrinsic fluorescence (Fig. 3a). The theranostic agent was employed to image and kill cancer cells expressing both somatostatin receptors and cathepsin B. In contrast, normal cells with low expression of somatostatin receptors and cathepsin B were not affected. The new dual-targeting theranostic agent has been proved effective in FLI-guided cancer CHT.

Following this idea, Perez and co-workers[66] developed an activatable targeted small molecule-based theranostic agent Doxo-S-S-Fol. Such a nanosystem is composed of a folate
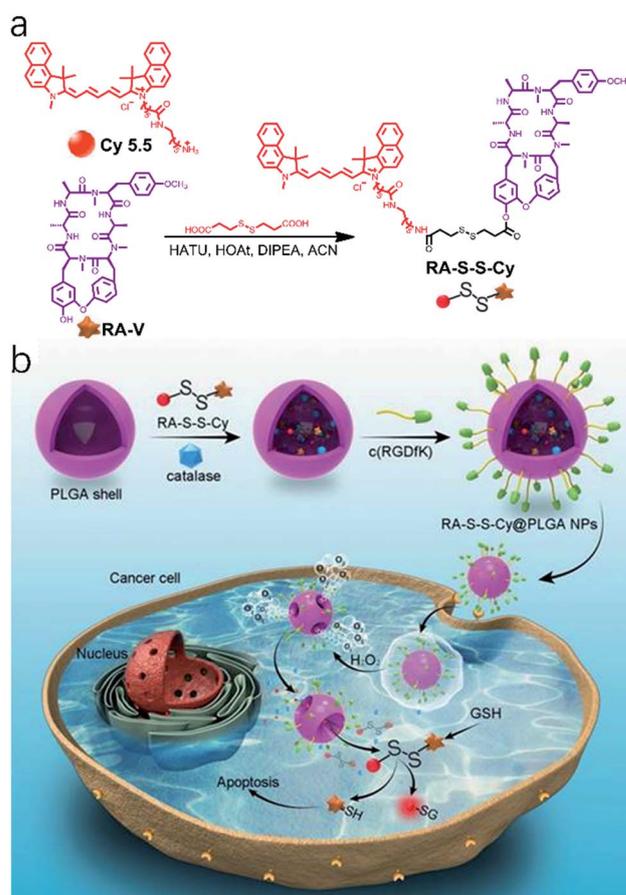

Fig. 4 (a) Synthesis route to the activatable RA-S-S-Cy prodrug. (b) Schematic illustration of the RA-S-S-Cy@PLGA NP structure and the mechanism of cytotoxicity and fluorescence enhancement produced by RA-S-S-Cy@PLGA NPs upon exposure to GSH. Adapted from ref. 75. Copyright© Ivyspring International Publisher.

receptor which is highly expressed in various solid tumors, a disulfide linker cleavable by glutathione (GSH) or thioredoxin (Trx) which are relatively abundant in tumor cells, and DOX, a fluorescent antitumor drug (Fig. 3b and c). Doxo-S-S-Fol was activated *via* disulfide-cleavage in the presence of intracellular reduced GSH, showing enhanced fluorescence and cellular toxicity only in folate-receptor positive cells and exhibiting extremely low toxicity to cells that do not express the receptor. The results presented in this work have the potential to guide the development of AMAs, thus establishing imaging of drug distribution, drug activation, and therapeutic efficacy.

Because of major limitations such as low biological availability, multi-drug resistance, and high systemic toxicity,[74] traditional chemotherapeutic agents are severely restricted in clinical applications. Nanoparticles used as drug carriers provide new opportunities to increase solubility, prolong bioavailability, reduce side effects, target drug delivery, and combat multi-drug resistance for cancer therapy.[75,76] Following this idea, a theranostic nanosystem (RA-S-S-Cy@PLGA NPs) with redox dual-activation and O_2-evolution was developed by Tan and co-workers.[77] The natural homodicyclohexapeptide deoxybouvardin (RA-V) as the active anti-tumor agent, a near-infrared (NIR) fluorescent dye Cy5.5 as the fluorophore to monitor the activation of RA-V, and a disulfide bond as a thiol-specific cleavable linker were covalently bonded to form the theranostic agent (RA-S-S-Cy). And RA-S-S-Cy@PLGA NPs were constructed by loading a theranostic agent RA-S-S-Cy and an O_2-generating agent catalase onto D,L-lactic-co-glycolic acid (PLGA) nanoparticles that were conjugated with a tumor-targeting cyclic pentapeptide c(RGDfK)[78] (Fig. 4a). The theranostic nano agent modified with c(RGDfK) was endocytosed into the targeted cancer cells *via* $\alpha_v\beta_3$ integrin-mediated internalization. Then, a high level of intracellular H_2O_2 in $\alpha_v\beta_3$ integrin-rich cancer cells penetrated the RA-S-S-Cy@PLGA NPs, leading to a huge amount of oxygen produced. The PLGA shell wall was instantly disrupted by O_2 bubbles, leading to the release of RA-S-S-Cy. As such, RA-V was released in a cell-specific and redox dual-activatable manner, leading to cellular apoptosis and enhanced NIR fluorescence (Fig. 4b). Moreover, RA-S-S-Cy@PLGA NPs were successfully applied to monitor drug release and chemotherapeutic efficacy *in vivo*. As a result, the nano platform provides a potential tool for a profound understanding of drug release mechanisms and the chemotherapy process.

2.2. Photoacoustic imaging (PAI)-guided chemotherapy (CHT)

PAI, also known as optoacoustic imaging, is currently one of the burgeoning biomedical imaging techniques.[79,80] In comparison with traditional optical imaging which suffers from shallow tissue penetration depth,[81] molecular PAI which combines NIR laser excitation with ultrasonic detection can provide high
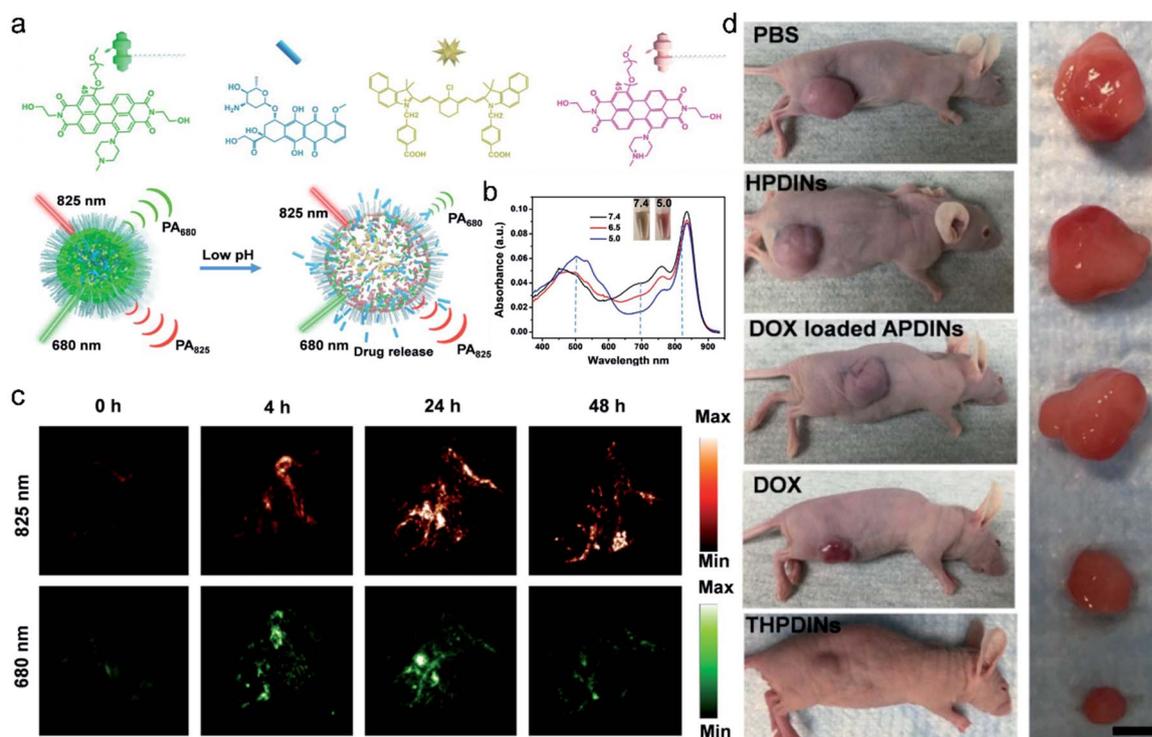

Fig. 5 (a) Schematic illustration of the sensing and drug release mechanism of THPDINs. The THPDINs are self-assembled with pH-sensitive HPDI (green), an anticancer drug of DOX (blue), and a pH-inert IR825 (gold). (b) UV-vis absorption spectra of THPDINs. (c) *In vivo* PA imaging of tumor pH. Representative PA images of a subcutaneous U87MG tumor in a nude mouse after intravenous administration of the THPDINs at post-injection times of 0, 4, 24, and 48 h. (d) Representative photographs of tumor-bearing mice with resected U87MG tumors in different treatment groups on day 18. Adapted from ref. 81. Copyright© Ivyspring International Publisher.

spatial resolution mapping in deep tissues (≈12 cm) while retaining the high contrast of optical imaging to guide accurate theranostics.[80,82,83] Although activatable photoacoustic probes have the capability of imaging cancer-specific biomarkers, the effective drug delivery and drug release monitoring are hampered due to the limitations of their molecular structures. Hence, for theranostic agents, contrast agents with a high molar absorbance (extinction) coefficient and low non-radiative quantum yield in the near-infrared region are urgently needed.[84]

Recently, multifunctional nano theranostics prepared by nanoparticle encapsulation for real-time ratiometric PA imaging of the tumor acidic pH and monitoring of drug release in living mice were developed by Chen et al.[85] The theranostic platform (THPDINs) was first constructed by self-assembly of acid-responsive amine-substituted PDI, a pH irrelevant IR825 dye, and the anti-cancer drug DOX (Fig. 5a). The typical small semiconducting molecule of PDI showed a blueshift of its absorption from 680 nm to 530 nm in an acidic environment (Fig. 5b), which caused a reduction in the photoacoustic signals of PDI at 680 nm. Also, in the mild acidic tumor microenvironment, the THPDINs were induced to form a loosened nanostructure that could accelerate the release of the encapsulated DOX together with PA signals weakened at 680 nm. Meanwhile, acting as an internal reference, IR825 still remained the same including its chemical structure and characteristic PA signal at 825 nm (Fig. 5c). Moreover, the antitumor efficacy of the THPDINs was also evaluated in U87MG tumor mice (Fig. 5d). The mice treated with other contrast reagents such as PBS, HPDINs, and DOX-loaded APDINs, exhibited rapid tumor growth, and those treated with free DOX showed slower tumor growth. THPDINs could effectively inhibit tumor growth. Besides, no remarkable body weight loss was observed. These results indicated that the theranostic platform of THPDINs showed high anti-cancer effects, good biocompatibility, and few side effects. This strategy will provide a reference for the development of smart activatable theranostic nanoplatforms and will greatly promote the application of PA-guided chemotherapy in biology and medicine.

3. Phototheranostics

Phototherapy,[8] mainly including PDT and PTT, has gained considerable attention in cancer therapy owing to its features of minimal invasiveness, rapid treatment, high temporal–spatial controllability and low systemic toxicity. In general, both PDT and PTT need the accumulation of phototherapeutic agents in the tumor site and subsequently pinpoint light irradiation with the corresponding wavelength. PDT mainly consists of three indispensable elements: a photosensitizer, excitation light, and oxygen molecules in tumor tissues.[86] Upon light irradiation with specific wavelengths, the photosensitizers convert molecular oxygen into cytotoxic ROS (such as $^1O_2$, $\cdot OH$, and $O_2 \cdot^-$) after absorbing NIR photons, which enable the destruction of cancer cells through oxidative stress and therefore induce apoptosis. Activatable PDT could enhance the selectivity of cancer therapy through introducing modified photosensitizers with a bio-

responsive element, which was unable to produce ROS even upon irradiation. Only activation to ultimately restore the native photosensitizers can produce cytotoxic ROS under light irradiation. As a result, global irradiation can cause only cancer cells to die leaving healthy cells unharmed, thereby minimizing side effects. Also, activatable PTT employs phototherapy agents with photothermal conversion ability only when stimulated by tumor markers, which transform external light energy into heat, causing a temperature increase at the tumor site and destroying the function of cancer cells, hence achieving the purpose of antitumor treatment. Benefiting from high tumor specificity, a short irradiation time, a rapid treatment process, repeatable operability, no drug resistance, and a good therapeutic effect, activatable PDT and PTT have the potential to be independent cancer treatment methods, respectively, and numerous novel theranostic agents combining optical imaging with phototherapy have recently been developed.[5,6,87–89]

3.1. Fluorescence imaging-guided PDT

With respect to FLI-guided therapy, the selection of high specificity activatable theranostic agents with excellent optical
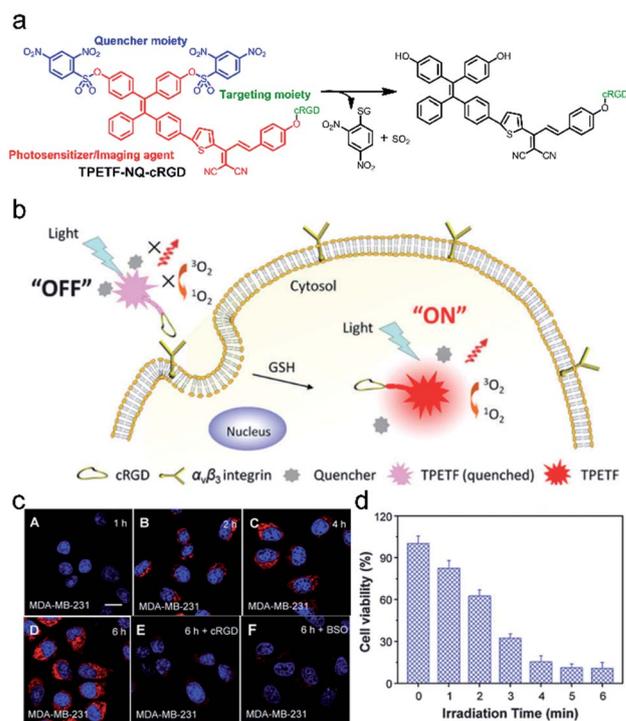

Fig. 6 (a) Schematic illustration of the probe TPETF-NQ-cRGD activated by glutathione (GSH) to release the photosensitizer. (b) The probe remains in the "off" state which is non-fluorescent with almost no ROS generation upon light irradiation, but the fluorescence and ROS generation can be turned "on" after receptor mediated endocytosis, followed by intracellular GSH activation. (c) Confocal laser scanning microscope images of MDA-MB-231 cells pre-incubated with cRGD (E) or BSO (F) and further incubated with TPETF-NQ-cRGD (10 mM) for 1 h (A), 2 h (B), 4 h (C), and 6 h (D). (d) Cytotoxicity of the probe to MDA-MB-231 cells with different time durations of light irradiation. Adapted from ref. 86. Copyright© 2016 Royal Society of Chemistry.
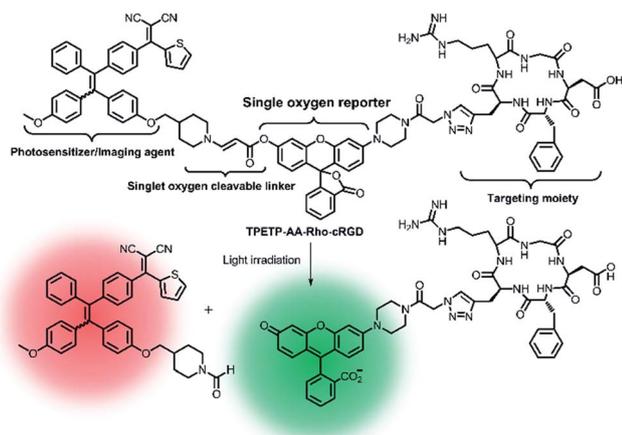
Fig. 7 Schematic representation of the proposed singlet oxygen self-reporting mechanism. Adapted from ref. 85. Copyright© 2016 Royal Society of Chemistry.

properties is a great challenge for PDT in cancer treatment. Recently, a special kind of photosensitizer with an aggregation-induced emission (AIE) character has been successfully developed for PDT,[14,90–92] because these AIEgens can emit signals in the whole visible range, even in the NIR region and have been demonstrated to be highly efficient ROS generators as aggregates.[87,93] Taking advantage of these mentioned features, a novel bio-probe TPETF-NQ-cRGD was developed by Liu and co-workers.[92] The probe, composed of a tetraphenylethylene moiety with AIE properties as an imaging agent, biothiol cleavable 2,4-dinitrobenzenesulfonyl (NQ) as a quencher moiety, and a cyclic arginine–glycine–aspartic acid (cRGD) tripeptide as a targeting group of $\alpha_v\beta_3$ integrin overexpressed in cancer cells, can specifically recognize and ablate cancer cells (Fig. 6a and b). The fluorescence and photosensitizing activity of TPETF-NQ-cRGD was quenched in the aggregated state. After TPETF-NQ-cRGD enters the $\alpha_v\beta_3$ integrin–GSH dual-overexpressed cancer cells by endocytosis, high brightness emission from the probe appeared, followed by rapid apoptosis of the cells (Fig. 6c and d), which is due to the release of the quencher moiety NQ from the probe and the generation of a large amount of ROS, especially singlet oxygen ($^1O_2$). However, almost no signals were observed in cells pretreated with cRGD as an $\alpha_v\beta_3$ integrin blocker or BSO as an endogenous GSH inhibitor. This work clearly demonstrates that both recognition and ablation of cancer cells are realized by FLI-guided PDT.

Later on, a theranostic agent TPETP-AA-Rho-cRGD (Fig. 7) containing cRGD, an $^1O_2$-responsive green-emissive fluorogenic rhodol moiety, an $^1O_2$-cleavable linker aminoacrylate (AA), and
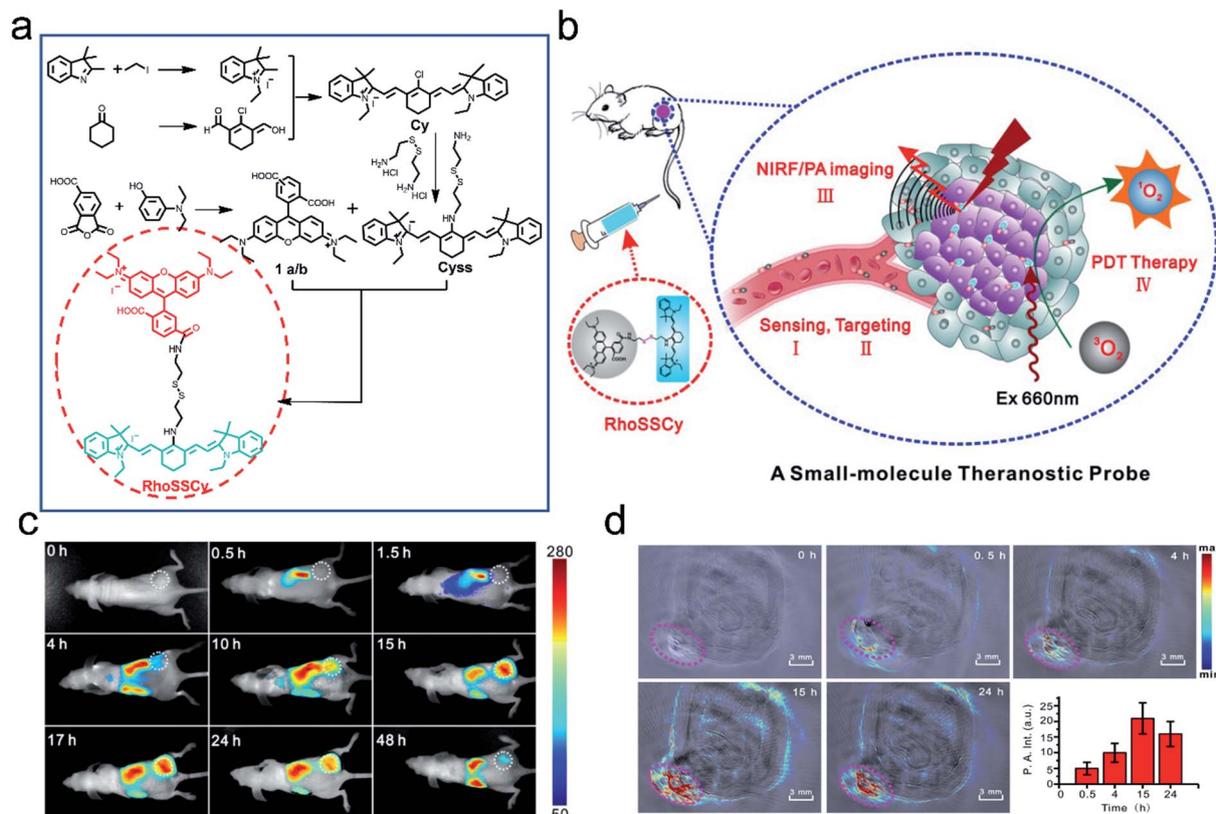

Fig. 8 Illustration of the synthesis and functions of RhoSSCy. (a) Synthetic scheme of the probe RhoSSCy. (b) Illustration of the theranostic mechanism of RhoSSCy. (c) NIRF imaging of tumors (white circle) in living mice at different time intervals after injection of RhoSSCy. (d) PA images of a tumor bearing nude mouse. The pink circle indicated the location of the tumor. Insert: semiquantitative fluorescence intensity of the tumor at indicated time points. Adapted from ref. 93. Copyright© Ivyspring International Publisher.

a red-emissive AIE-active unit (TPETP) was successfully designed by the same group.[91] The probe TPETP-AA-Rho-cRGD can emit red fluorescence from the TPETP moiety in aqueous solution, which endows it with the ability to track itself. The cRGD with the targeting function enabled TPETP-AARho-cRGD to specifically target $\alpha_v\beta_3$-overexpressing cancer cells. Upon imaging-guided light irradiation, the DA-MB-231 cancer cells were quickly killed by $^1O_2$ which was rapidly produced by TPETP. Besides, the AA linker was efficiently cleaved by $^1O_2$, leading to an obvious green fluorescence from rhodol. This probe design thus represented an advanced strategy for real-time *in situ* monitoring of ROS production during PDT through self-tracking.

3.2. Fluorescence and photoacoustic imaging-guided PDT

Since each imaging modality (FL, PA, PET, MRI, *etc.*) has its advantages and limitations, dual-mode or multi-mode imaging techniques are often used to collect complementary information to verify the diagnosis.[94,95] As we all know, fluorescence imaging possesses high sensitivity and outstanding resolution, but it suffers from low penetration depth, while PA can provide desirable tissue penetration depth. As such, a diagnostic probe with FL and PA dual modalities could provide much more precise information and has great potential for biological applications.[82,96–98]

Cai *et al.*[99] developed the first small-molecule "Four in One" theranostic probe RhoSSCy which integrates tumor targeting, pH/thiol detection, near-infrared fluorescence (NIRF)/PA dual-modal imaging, and PDT therapy (Fig. 8a and b). The probe

was constructed using heptamethine cyanine IR765 (Cy) and 5′-carboxyrhodamine (Rho) *via* a cystamine linker. In the probe, the reducible disulfide and amino group acted as the thiol recognition group and pH tunable sensor, respectively. *In vitro* experiments demonstrated that the probe could quantitatively analyze and image intracellular thiols and the pH gradient with high sensitivity. Moreover, the probe exhibited splendid tumor-targeting and accumulation, which was verified by near-infrared fluorescence (NIRF) and photoacoustic (PA) dual-modal imaging of tumors (Fig. 8c and d). Significantly, RhoSSCy could generate ROS in tumors upon dual-mode imaging-guided light irradiation and achieve robust antitumor activity through PDT. Such AMAs have great potential in precision detection and efficient treatment of tumors.

3.3. Chemiluminescence imaging-guided PDT

Chemiluminescence, a phenomenon of light radiation accompanied by chemical reactions, has been increasingly recognized as a powerful tool for disease diagnosis and biological analysis.[100–102] Compared to traditional fluorescence imaging, CLI has the advantages of high sensitivity, low phototoxicity, and high signal-to-noise ratio due to the removal of the external excitation source. Peroxalate derivatives working as light-emitting functionalities have been widely explored for chemiluminescence. They can be oxidized by hydrogen peroxide (H_2O_2) to form a high-energy and unstable dioxetanedione, which is an active chemiluminescent substrate that spontaneously undergoes decomposition to emit photons and the energy
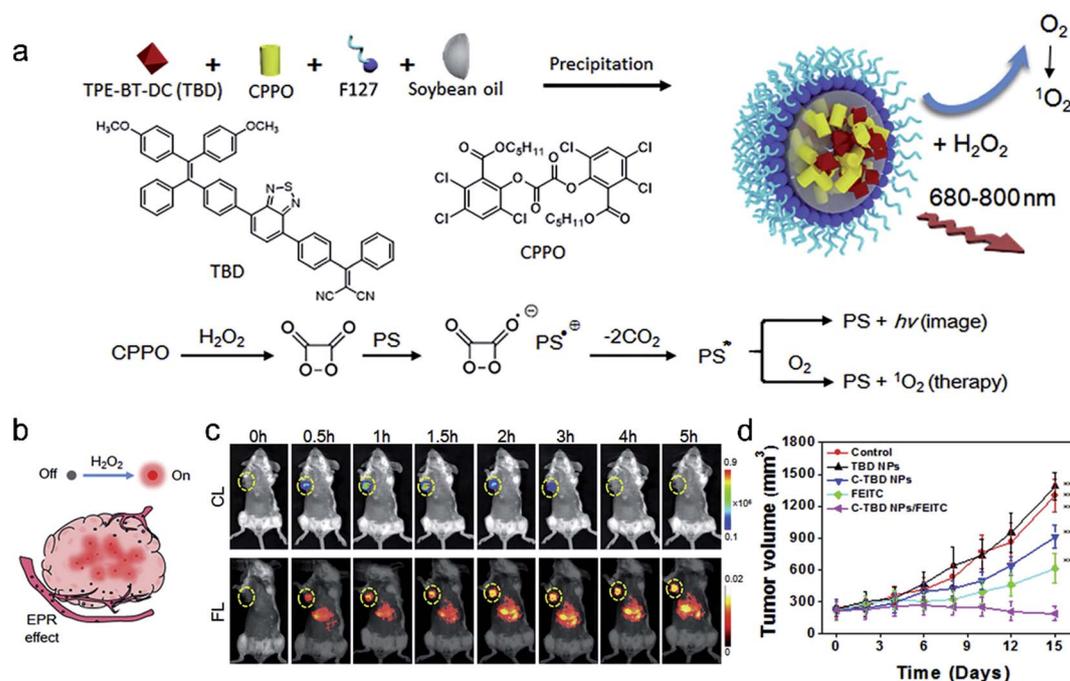

Fig. 9 (a) The preparation of C-TBD NPs and illustration of the principle for chemiluminescence and $^1O_2$ generation of C-TBD NPs in the presence of H_2O_2. (b) Schematic illustration of activated C-TBD NPs to image tumors within the H_2O_2-enriched tumor microenvironment. (c) Time-dependent *in vivo* chemiluminescence (top) and fluorescence (bottom) images of mice injected with C-TBD NPs (1 mg mL^{-1} based on C-TBD, 100 mL per mouse) over 5 h periods. Tumor regions are marked with yellow circles. (d) Tumor growth curves with different therapies. Adapted from ref. 99. Copyright© 2017 Elsevier.

is transferred to a nearby fluorescent dye, leading to a particular optical signal. Based on this, chemiluminescence can be used as an appropriate imaging method for specific tumor imaging due to a higher amount of H_2O_2 in solid tumors than in normal tissues,[103] and it is widely used as a guiding technique in photodynamic therapy.[104,105]

Encouraged by the great properties of chemiluminescence, Liu et al.[105] developed a novel therapeutic agent that was based on CLI-guided PDT for accurate diagnosis and treatment of cancer. The therapeutic agent C-TBD nanoparticles (C-TBD NPs) were composed of bis[2,4,5-trichloro-6-(pentyloxycarbonyl) phenyl] oxalate (CPPO) as the chemical excitation source and TBD as the high efficiency photosensitizer with the capability of FR/NIR emission and ROS production, soybean oil as the retarder, and pluronic F127 as the encapsulating agent (Fig. 9a). In this nanosystem, a high-energy 1,2-dioxetanedione intermediate, formed from CPPO with the action of H_2O_2, can excite TBD through a chemically initiated electron exchange luminescence (CIEEL) process. Finally, the excited TBD can generate luminescence and react with oxygen to generate $^1O_2$ without an extra light source, which provides a novel strategy in tumor imaging and treatment. The in vivo experiments demonstrated that C-TBD NPs could specifically track tumors through chemiluminescence imaging. In contrast, fluorescence signals in both the tumor and the reticuloendothelial system (RES) organs (such as the liver) were observed (Fig. 9b and c). Besides, compared with the other control groups, the tumors of mice treated with both C-TBD NPs and the H_2O_2 enhancing agent β-phenylethyl isothiocyanate (FEITC) exhibited the most significant growth inhibition (Fig. 9d), verifying the effectiveness of the combination therapy. This work presents a novel strategy for CLI-guided PDT, which can motivate more research on tumor diagnosis and treatment.

3.4. Fluorescence imaging-guided CHT and PDT

Materials based on a single mode therapy may not be able to match the complex biological environment effectively due to their limited functions.[106,107] Therefore, the design of dual-mode or multi-mode therapy materials has become a new development trend. Imaging-guided chemo-photodynamic dual-mode therapy is a novel modality of cancer theranostics, which can improve therapeutic efficiency with minimized side effects and avoid the burden of multiple injections of different therapeutic agents in clinical applications.[8,108,109] Liu and co-workers[20] developed a kind of theranostic agent (Co-NPs) which was constructed by self-assembly of a paclitaxel (PTX,[110] an anti-tumor drug for ovarian and breast cancer) dimer and two-photo photosensitizer (Fig. 10a). Upon short light irradiation, an increasing bright fluorescence signal from Co-NPs in the lysosome was observed, which was ascribed to the photochemical internalization (PCI) effect, leading to an enhanced cellular uptake. Then, Co-NPs escaped from the lysosome into the cytoplasm after 808 nm laser irradiation, which was proved by the lysosome colocalization experiment. Synchronously, $^1O_2$ was generated by the photo-activation of the photosensitizer 2PE-PS in Co-NPs, thus

killing the cells by PDT. In the presence of GSH, the disulfide bond in the PTX dimer was cleaved and the paclitaxel monomer was released. The free PTX diffused to the cytosol for chemotherapy (Fig. 10b). Hence, the combination CHT–PDT pathway based on fluorescence molecular theranostic agents had great potential for cancer theranostics.

3.5. Fluorescence and photoacoustic imaging-guided PTT

PTT which requires efficient conversion of photon energy into heat follows the principle of PA imaging.[40,111] Significantly, PTT has advantages over PDT in terms of cancer therapy, such as the therapeutic efficiency of PTT being frequently higher than that of PDT and PTT working well in a hypoxic tumor environment. Hence, the combination of fluorescence/photoacoustic imaging and photothermal therapy proved to be an eminent modality in cancer theranostics and can be used not only for accurate diagnosis of tumors but also for ablating tumors.

Based on these characteristics, Cai et al.[12] developed pH-sensitive theranostic agents for precision detection and efficient therapy of tumors (Fig. 11a). IR-PY was composed of a NIRF heptamethine cyanine dye IR-822, which possessed high extinction coefficients and native preferential tumor accumulation properties, and N^1-(pyridin-4-ylmethyl)ethane-1,2-diamine (PY) as a pH-sensing receptor. In an acidic tumor microenvironment, the NIR fluorescence emission intensity (at 765 nm) of IR-PY increased due to the inhibition of the photo-induced electron-transfer process, which allowed the probe IR-PY to exhibit high spatial resolution for PAI in the tumor and effective tumor photothermal ablation in vivo. Upon NIR 808 nm laser irradiation, the tumors in mice were remarkably ablated through PTT (Fig. 11b). The "all in one" multifunctional agent has extensive clinical prospects in NIRF/PA dual-modal imaging-guided cancer diagnosis and treatment.

Recently, an activatable theranostic probe for imaging-guided therapy has been developed by our group.[9] The probe CyGal-P was designed by attaching a D-galactose moiety on
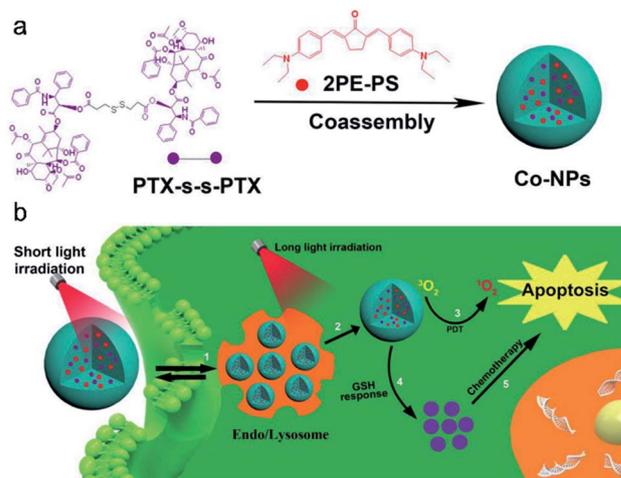

Fig. 10 (a) Preparation of nanoparticles. (b) Schematic illustration of the synergistic CHT and PDT. Adapted from ref. 20. Copyright© 2019 Elsevier.
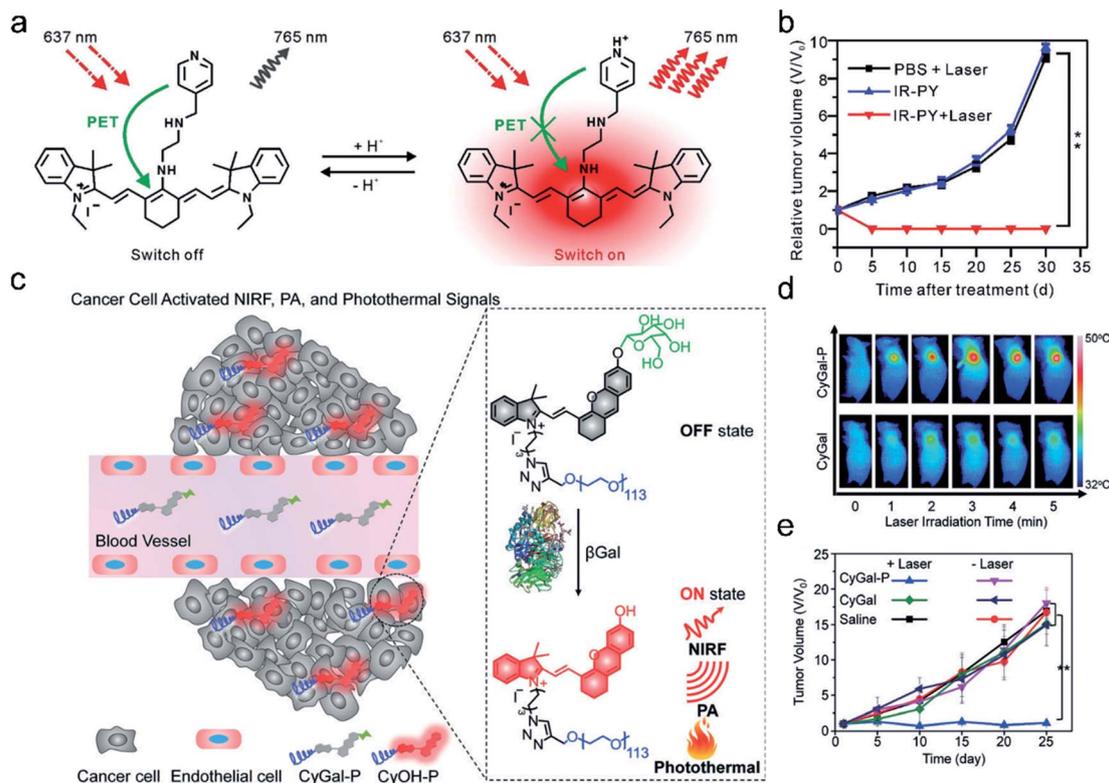
Fig. 11 (a) Schematic illustration of IR-PY as a versatile theranostic probe for pH sensing, tumor targeting, and NIRF/PA dual-modal imaging-guided PTT therapy. (b) The tumor growth curve for 30 days post-treatment for the different groups. Adapted from ref. 12. Copyright© 2017 Royal Society of Chemistry. (c) Schematic illustration of the activation mechanism of the macrotheranostic probe CyGal-P in βGal-over-expressing cancer cells. (d) Infrared thermal images of SKOV3 tumor-bearing mice under laser irradiation for different durations after intravenous injection of CyGal-P and CyGal. (e) Tumor growth curves of mice after intravenous injection of saline, CyGal, and CyGal-P into SKOV3 tumor-bearing mice with or without laser irradiation at 680 nm. Adapted from ref. 9. Copyright© 2018 Wiley-VCH Verlag GmbH & Co. KGaA, Weinheim.

a NIR chromophore CyOH, which was linked by a long PEG chain as a hydrophilic group to promote in vivo biodistribution (Fig. 11c). CyGal-P initially exhibited non-fluorescence and non-photoacoustic signals. In the presence of β-galactosidase (β-Gal) which is overexpressed in primary ovarian cancer cells, NIRF, PA and the photothermal properties of CyGal-P were switched on, which was confirmed by NIRF and PA imaging in the tumors. In contrast, the control probe CyGal without conjugation of the PEG chain did not exhibit observable NIRF, PA and photothermal signals in the tumors (Fig. 11d). Moreover, CyGal-P could effectively suppress cancer growth upon laser irradiation (Fig. 11e) and no obvious histopathological abnormalities were found in normal tissues. This study thus offers a new approach towards activatable multimodal imaging-guided PTT.

4. Conclusion

Theranostics has advantages in improving the treatment effect of cancer and reducing side effects. Hence, the development of effective theranostic agents is of vital importance in cancer therapy and evaluation of the therapeutic efficacy. In this perspective, we have focused on the development of AMAs. The main design concept of current AMAs is to integrate imaging agents, analyte-specific cleavable linkers, therapeutic agents,

and targeting groups. The "all-in-one" approach that combines different functional components in one platform has obvious advantages over a single modality of diagnosis or treatment because it can reduce side effects and minimize the probability of over-medication in tumor therapy. However, it also faces some problems that need to be solved: (i) small molecules often encounter photobleaching issues under prolonged exposure, making AMAs less favorable for long-term clinical applications. In addition, the structures of AMAs are more complicated than those of normal photosensitizers. Hence, design of photostable imaging reagents with simple synthetic procedures is needed.[87] (ii) How to improve the specific uptake of theranostic agents in tumor tissues is another question. Due to the high permeability of AMAs, they have poor enrichment capacity in the tumor area, leading to a low therapeutic effect. Hence, it is necessary to optimize the targeting ability of AMAs and use various specific targeting molecules or proteins to enhance the targeting effect of AMAs on tumor sites. (iii) The therapeutic performance of AMAs needs to be improved. Previous research[54] has shown that single therapy often has a limited therapeutic effect on tumors, while synergistic therapy can achieve the curative effect of "1 + 1 > 2", which can overcome tumor tolerance to single therapy. As for imaging, in the primary tumor and metastases for early diagnosis and therapy applications, various imaging modes

have advantages and application scope. Multi-mode imaging (such as FLI, PAI, and CLI) can overcome the false positives that may be caused by single-mode imaging and improve the accuracy of imaging and detection. Therefore, multi-mode imaging can achieve complementary advantages and better imaging results.

Nowadays, with the development of material technology, nanomedicine, and bioengineering, the integration of diagnosis and treatment will provide new opportunities for mankind to conquer cancer.

Conflicts of interest

There are no conflicts to declare.

Acknowledgements

Notes and references

1 R. L. Siegel, K. D. Miller and A. Jemal, *Ca-Cancer J. Clin.*, 2019, **69**, 7–34.

2 C. Sawyers, *Nature*, 2004, **432**, 294–297.

3 I. Brigger, C. Dubernet and P. Couvreur, *Adv. Drug Delivery Rev.*, 2012, **64**, 24–36.

4 G. Feng and B. Liu, *Small*, 2016, **12**, 6528–6535.

5 F. Wang, J. Xiao, S. Chen, H. Sun, B. Yang, J. Jiang, X. Zhou and J. Du, *Adv. Mater.*, 2018, **30**, 1705674.

6 W. Fan, W. Bu and J. Shi, *Adv. Mater.*, 2016, **28**, 3987–4011.

7 R. Kumar, W. S. Shin, K. Sunwoo, W. Y. Kim, S. Koo, S. Bhuniya and J. S. Kim, *Chem. Soc. Rev.*, 2015, **44**, 6670–6683.

8 H. Zhu, P. Cheng, P. Chen and K. Pu, *Biomater. Sci.*, 2018, **6**, 746–765.

9 X. Zhen, J. Zhang, J. Huang, C. Xie, Q. Miao and K. Pu, *Angew. Chem., Int. Ed.*, 2018, **57**, 7804–7808.

10 D. Yao, S. Yang, Y. Wang, K. Bian, W. Yang, D. Wang and B. Zhang, *Nanoscale*, 2019, **11**, 6307–6314.

11 X. Meng, J. Zhang, Z. Sun, L. Zhou, G. Deng, S. Li, W. Li, P. Gong and L. Cai, *Theranostics*, 2018, **8**, 6025–6034.

12 X. Meng, W. Li, Z. Sun, J. Zhang, L. Zhou, G. Deng, P. Gong and L. Cai, *J. Mater. Chem. B*, 2017, **5**, 9405–9411.

13 W. Lv, S. Chi, W. Feng, T. Liang, D. Song and Z. Liu, *Chem. Commun.*, 2019, **55**, 7037–7040.

14 Y. Yuan, C. J. Zhang, M. Gao, R. Zhang, B. Z. Tang and B. Liu, *Angew. Chem., Int. Ed.*, 2015, **54**, 1780–1786.

15 J. Qi, C. Chen, X. Zhang, X. Hu, S. Ji, R. T. Kwok, J. W. Lam, D. Ding and B. Z. Tang, *Nat. Commun.*, 2018, **9**, 1848.

16 K. Zhang, Y. Lv, J. Meng, J. Wang, A. Peng, X. Wang and Z. Tian, *Anal. Chim. Acta*, 2019, **1061**, 142–151.

17 J. Tian, L. Ding, H.-J. Xu, Z. Shen, H. Ju, L. Jia, L. Bao and J.-S. Yu, *J. Am. Chem. Soc.*, 2013, **135**, 18850–18858.

18 Q. Pei, X. Hu, X. Zheng, S. Liu, Y. Li, X. Jing and Z. Xie, *ACS Nano*, 2018, **12**, 1630–1641.

19 M. Xiao, W. Sun, J. Fan, J. Cao, Y. Li, K. Shao, M. Li, X. Li, Y. Kang, W. Zhang, S. Long, J. Du and X. Peng, *Adv. Funct. Mater.*, 2018, **28**, 1805128.

20 T. Zhang, L. Fu, X. Zheng, M. Liu, Q. Pei, X. Wang and S. Liu, *Dyes Pigm.*, 2019, **167**, 195–203.

21 J. Li, J. Rao and K. Pu, *Biomaterials*, 2018, **155**, 217–235.

22 J. Li, C. Xie, J. Huang, Y. Jiang, Q. Miao and K. Pu, *Angew. Chem., Int. Ed.*, 2018, **57**, 3995–3998.

23 Y. Lyu, Y. Fang, Q. Miao, X. Zhen, D. Ding and K. Pu, *ACS Nano*, 2016, **10**, 4472–4481.

24 Z. Wang, X. Zhen, P. K. Upputuri, Y. Jiang, J. Lau, M. Pramanik, K. Pu and B. Xing, *ACS Nano*, 2019, **13**, 5816–5825.

25 C. Xie, P. Cheng and K. Pu, *Chem. –Eur. J.*, 2018, **24**, 12121–12130.

26 X. Zhen, P. Cheng and K. Pu, *Small*, 2019, **15**, 1804105.

27 X. Zhen, C. Xie, Y. Jiang, X. Ai, B. Xing and K. Pu, *Nano Lett.*, 2018, **18**, 1498–1505.

28 X. Zhen, C. Xie and K. Pu, *Angew. Chem., Int. Ed.*, 2018, **57**, 3938–3942.

29 X. Zhen, J. Zhang, J. Huang, C. Xie, Q. Miao and K. Pu, *Angew. Chem., Int. Ed.*, 2018, **57**, 7804–7808.

30 H. Zhu, Y. Fang, Q. Miao, X. Qi, D. Ding, P. Chen and K. Pu, *ACS Nano*, 2017, **11**, 8998–9009.

31 H. Zhu, J. Li, X. Qi, P. Chen and K. Pu, *Nano Lett.*, 2017, **18**, 586–594.

32 J. Zhang, P. Cheng and K. Pu, *Bioconjugate Chem.*, 2019, **30**, 2089–2101.

33 T. D. MacDonald, T. W. Liu and G. Zheng, *Angew. Chem., Int. Ed.*, 2014, **53**, 6956–6959.

34 S. Liu, X. Zhou, H. Zhang, H. Ou, J. W. Y. Lam, Y. Liu, L. Shi, D. Ding and B. Z. Tang, *J. Am. Chem. Soc.*, 2019, **141**, 5359–5368.

35 J. F. Lovell, C. S. Jin, E. Huynh, H. Jin, C. Kim, J. L. Rubinstein, W. C. W. Chan, W. Cao, L. V. Wang and G. Zheng, *Nat. Mater.*, 2011, **10**, 324–332.

36 Y. Cai, W. Si, W. Huang, P. Chen, J. Shao and X. Dong, *Small*, 2018, **14**, 1704247.

37 G. Jin, R. He, Q. Liu, M. Lin, Y. Dong, K. Li, B. Z. Tang, B. Liu and F. Xu, *Theranostics*, 2019, **9**, 246–264.

38 Y. Liu, Y. Liu, W. Bu, C. Cheng, C. Zuo, Q. Xiao, Y. Sun, D. Ni, C. Zhang and J. Liu, *Angew. Chem., Int. Ed.*, 2015, **54**, 8105–8109.

39 C. Liang, S. Diao, C. Wang, H. Gong, T. Liu, G. Hong, X. Shi, H. Dai and Z. Liu, *Adv. Mater.*, 2014, **26**, 5646–5652.

40 L. Dykman and N. Khlebtsov, *Chem. Soc. Rev.*, 2012, **41**, 2256–2282.

41 J. T. Robinson, S. M. Tabakman, Y. Liang, H. Wang, H. Sanchez Casalongue, D. Vinh and H. Dai, *J. Am. Chem. Soc.*, 2011, **133**, 6825–6831.

42 X.-H. Peng, X. Qian, H. Mao and A. Y. Wang, *Int. J. Nanomed.*, 2008, **3**, 311–321.

43 R. Savla, O. Taratula, O. Garbuzenko and T. Minko, *J. Controlled Release*, 2011, **153**, 16–22.

44 Y. Lyu, J. Zeng, Y. Jiang, X. Zhen, T. Wang, S. Qiu, X. Lou, M. Gao and K. Pu, *ACS Nano*, 2018, **12**, 1801–1810.

45 D. Cui, J. Huang, X. Zhen, J. Li, Y. Jiang and K. Pu, *Angew. Chem., Int. Ed.*, 2019, **58**, 5920–5924.

46 Y. Jiang, D. Cui, Y. Fang, X. Zhen, P. K. Upputuri, M. Pramanik, D. Ding and K. Pu, *Biomaterials*, 2017, **145**, 168–177.

47 Y. Jiang, J. Li, Z. Zeng, C. Xie, Y. Lyu and K. Pu, *Angew. Chem., Int. Ed.*, 2019, **58**, 8161–8165.

48 Y. Jiang, J. Li, X. Zhen, C. Xie and K. Pu, *Adv. Mater.*, 2018, **30**, 1705980.

49 J. Li, X. Zhen, Y. Lyu, Y. Jiang, J. Huang and K. Pu, *ACS Nano*, 2018, **12**, 8520–8530.

50 S. Bhuniya, S. Maiti, E.-J. Kim, H. Lee, J. L. Sessler, K. S. Hong and J. S. Kim, *Angew. Chem., Int. Ed.*, 2014, **53**, 4469–4474.

51 P. Cheng, J. Zhang, J. Huang, Q. Miao, C. Xu and K. Pu, *Chem. Sci.*, 2018, **9**, 6340–6347.

52 J. Huang, J. Li, Y. Lyu, Q. Miao and K. Pu, *Nat. Mater.*, 2019, **18**, 1133–1143.

53 C. Wang, L. Cheng and Z. Liu, *Biomaterials*, 2011, **32**, 1110–1120.

54 W. Fan, B. Yung, P. Huang and X. Chen, *Chem. Rev.*, 2017, **117**, 13566–13638.

55 H.-B. Cheng, Y. Cui, R. Wang, N. Kwon and J. Yoon, *Coord. Chem. Rev.*, 2019, **392**, 237–254.

56 D. Zaak, R. Sroka, W. Khoder, C. Adam, S. Tritschler, A. Karl, O. Reich, R. Knuechel, R. Baumgartner, D. Tilki, G. Popken, A. Hofstetter and C. G. Stief, *Urology*, 2008, **72**, 345–348.

57 A. Wiehe, Y. M. Shaker, J. C. Brandt, S. Mebs and M. O. Senge, *Tetrahedron*, 2005, **61**, 5535–5564.

58 M. Kriegmair, R. Baumgartner, W. Lumper, R. Waidelich and A. Hofstetter, *Br. J. Urol.*, 1996, **77**, 667–671.

59 Y. Tian, S. Li, J. Song, T. Ji, M. Zhu, G. J. Anderson, J. Wei and G. Nie, *Biomaterials*, 2014, **35**, 2383–2390.

60 M. Berrada, A. Serreqi, F. Dabbarh, A. Owusu, A. Gupta and S. Lehnert, *Biomaterials*, 2005, **26**, 2115–2120.

61 S. D. Williams, R. Birch, L. H. Einhorn, L. Irwin, F. A. Greco and P. J. Loehrer, *N. Engl. J. Med.*, 1987, **316**, 1435–1440.

62 X. Dai, G. Guo, P. Zou, R. Cui, W. Chen, X. Chen, C. Yin, W. He, R. Vinothkumar, F. Yang, X. Zhang and G. Liang, *J. Exp. Clin. Cancer Res.*, 2017, **36**, 120.

63 K. Nakatomi, M. Yoshikawa, M. Oka, Y. Ikegami, S. Hayasaka, K. Sano, K. Shiozawa, S. Kawabata, H. Soda, T. Ishikawa, S. Tanabe and S. Kohno, *Biochem. Biophys. Res. Commun.*, 2001, **288**, 827–832.

64 A. N. Shah, J. M. Summy, J. Zhang, S. I. Park, N. U. Parikh and G. E. Gallick, *Ann. Surg. Oncol.*, 2007, **14**, 3629–3637.

65 J. P. MacKeigan, T. S. Collins and J. P.-Y. Ting, *J. Biol. Chem.*, 2000, **275**, 38953–38956.

66 S. Santra, C. Kaittanis, O. J. Santiesteban and J. M. Perez, *J. Am. Chem. Soc.*, 2011, **133**, 16680–16688.

67 R. Kumar, J. Han, H.-J. Lim, W. X. Ren, J.-Y. Lim, J.-H. Kim and J. S. Kim, *J. Am. Chem. Soc.*, 2014, **136**, 17836–17843.

68 J. Huang, Y. Wu, F. Zeng and S. Wu, *Theranostics*, 2019, **9**, 7313–7324.

69 M. H. Lee, J. Y. Kim, J. H. Han, S. Bhuniya, J. L. Sessler, C. Kang and J. S. Kim, *J. Am. Chem. Soc.*, 2012, **134**, 12668–12674.

70 Y.-H. Hsiang, L. F. Liu, M. E. Wall, M. C. Wani, A. W. Nicholas, G. Manikumar, S. Kirschenbaum, R. Silber and M. Potmesil, *Cancer Res.*, 1989, **49**, 4385–4389.

71 S. Maiti, N. Park, J. H. Han, H. M. Jeon, J. H. Lee, S. Bhuniya, C. Kang and J. S. Kim, *J. Am. Chem. Soc.*, 2013, **135**, 4567–4572.

72 S. Chen, X. Zhao, J. Chen, J. Chen, L. Kuznetsova, S. S. Wong and I. Ojima, *Bioconjugate Chem.*, 2010, **21**, 979–987.

73 X. Tian, K.-H. Baek and I. Shin, *Chem. Sci.*, 2013, **4**, 947–956.

74 P. Bhattarai, S. Hameed and Z. Dai, *Nanoscale*, 2018, **10**, 5393–5423.

75 W. Jiang, C. A. Von Roemeling, Y. Chen, Y. Qie, X. Liu, J. Chen and B. Y. Kim, *Nat. Biomed. Eng.*, 2017, **1**, 0029.

76 V. P. Chauhan and R. K. Jain, *Nat. Mater.*, 2013, **12**, 958–962.

77 H. Chen, F. Li, Y. Yao, Z. Wang, Z. Zhang and N. Tan, *Theranostics*, 2019, **9**, 90–103.

78 J. Wang, W. Li, Z. Lu, L. Zhang, Y. Hu, Q. Li, W. Du, X. Feng, H. Jia and B.-F. Liu, *Nanoscale*, 2017, **9**, 15598–15605.

79 V. Ntziachristos, J. Ripoll, L. V. Wang and R. Weissleder, *Nat. Biotechnol.*, 2005, **23**, 313–320.

80 L. V. Wang and S. Hu, *Science*, 2012, **335**, 1458–1462.

81 C. Xie, X. Zhen, Y. Lyu and K. Pu, *Adv. Mater.*, 2017, **29**, 1703693.

82 J. Zhang, X. Zhen, P. K. Upputuri, M. Pramanik, P. Chen and K. Pu, *Adv. Mater.*, 2017, **29**, 1604764.

83 U. Chitgupi, N. Nyayapathi, J. Kim, D. Wang, B. Sun, C. Li, K. Carter, W.-C. Huang, C. Kim, J. Xia and J. F. Lovell, *Adv. Mater.*, 2019, **31**, 1902279.

84 C. Kim, C. Favazza and L. V. Wang, *Chem. Rev.*, 2010, **110**, 2756–2782.

85 Z. Yang, J. Song, W. Tang, W. Fan, Y. Dai, Z. Shen, L. Lin, S. Cheng, Y. Liu, G. Niu, P. Rong, W. Wang and X. Chen, *Theranostics*, 2019, **9**, 526–536.

86 T. J. Dougherty, C. J. Gomer, B. W. Henderson, G. Jori, D. Kessel, M. Korbelik, J. Moan and Q. Peng, *J. Natl. Cancer Inst.*, 1998, **90**, 889–905.

87 D. Wang, M. M. S. Lee, W. Xu, R. T. K. Kwok, J. W. Y. Lam and B. Z. Tang, *Theranostics*, 2018, **8**, 4925–4956.

88 X. Li, S. Kolemen, J. Yoon and E. U. Akkaya, *Adv. Funct. Mater.*, 2017, **27**, 1604053.

89 J. F. Lovell, T. W. B. Liu, J. Chen and G. Zheng, *Chem. Rev.*, 2010, **110**, 2839–2857.

90 D. Wang, H. Su, R. T. Kwok, G. Shan, A. C. Leung, M. M. Lee, H. H. Sung, I. D. Williams, J. W. Lam and B. Z. Tang, *Adv. Funct. Mater.*, 2017, **27**, 1704039.

91 Y. Yuan, C.-J. Zhang, S. Xu and B. Liu, *Chem. Sci.*, 2016, **7**, 1862–1866.

92 Y. Yuan, S. Xu, C.-J. Zhang, R. Zhang and B. Liu, *J. Mater. Chem. B*, 2016, **4**, 169–176.

93 L. Yang, X. Wang, G. Zhang, X. Chen, G. Zhang and J. Jiang, *Nanoscale*, 2016, **8**, 17422–17426.

94 J. Kim, Y. Piao and T. Hyeon, *Chem. Soc. Rev.*, 2009, **38**, 372–390.

95 R. Bardhan, S. Lal, A. Joshi and N. J. Halas, *Acc. Chem. Res*, 2011, **44**, 936–946.

96 L. V. Wang, *Nat. Photonics*, 2009, **3**, 503–509.

97 C. Xie, P. K. Upputuri, X. Zhen, M. Pramanik and K. Pu, *Biomaterials*, 2017, **119**, 1–8.

98 Q. Miao and K. Pu, *Bioconjugate Chem.*, 2016, **27**, 2808–2823.

99 X. Meng, Y. Yang, L. Zhou, L. Zhang, Y. Lv, S. Li, Y. Wu, M. Zheng, W. Li, G. Gao, G. Deng, T. Jiang, D. Ni, P. Gong and L. Cai, *Theranostics*, 2017, **7**, 1781–1794.

100 T. H. Fereja, A. Hymete and T. Gunasekaran, *ISRN Spectrosc.*, 2013, **2013**, 230358.

101 N. Hananya and D. Shabat, *ACS Cent. Sci.*, 2019, **5**, 949–959.

102 A. Roda, P. Pasini, M. Mirasoli, E. Michelini and M. Guardigli, *Trends Biotechnol.*, 2004, **22**, 295–303.

103 H. Yuan, H. Chong, B. Wang, C. Zhu, L. Liu, Q. Yang, F. Lv and S. Wang, *J. Am. Chem. Soc.*, 2012, **134**, 13184–13187.

104 R. Chen, L. Zhang, J. Gao, W. Wu, Y. Hu and X. Jiang, *J. Biomed. Biotechnol.*, 2011, **2011**, 679492.

105 D. Mao, W. Wu, S. Ji, C. Chen, F. Hu, D. Kong, D. Ding and B. Liu, *Chem*, 2017, **3**, 991–1007.

106 P. García Calavia, I. Chambrier, M. J. Cook, A. H. Haines, R. A. Field and D. A. Russell, *J. Colloid Interface Sci.*, 2018, **512**, 249–259.

107 X. Yi, K. Yang, C. Liang, X. Zhong, P. Ning, G. Song, D. Wang, C. Ge, C. Chen, Z. Chai and Z. Liu, *Adv. Funct. Mater.*, 2015, **25**, 4689–4699.

108 A. Turksoy, D. Yildiz and E. U. Akkaya, *Coord. Chem. Rev.*, 2019, **379**, 47–64.

109 J. Li and K. Pu, *Chem. Soc. Rev.*, 2019, **48**, 38–71.

110 D. K. Armstrong, B. Bundy, L. Wenzel, H. Q. Huang, R. Baergen, S. Lele, L. J. Copeland, J. L. Walker and R. A. Burger, *N. Engl. J. Med.*, 2006, **354**, 34–43.

111 J. Yu, C. Yang, J. Li, Y. Ding, L. Zhang, M. Z. Yousaf, J. Lin, R. Pang, L. Wei and L. Xu, *Adv. Mater.*, 2014, **26**, 4114–4120.